

The role of atmospheric heat transport and regional feedbacks in the Arctic warming at equilibrium

Masakazu Yoshimori¹  · Ayako Abe-Ouchi^{2,3,4} · Alexandre Laîné^{2,3}

Received: 30 September 2016 / Accepted: 3 January 2017 / Published online: 18 January 2017
© Springer-Verlag Berlin Heidelberg 2017

Abstract It is well known that the Arctic warms much more than the rest of the world even under spatially quasi-uniform radiative forcing such as that due to an increase in atmospheric CO₂ concentration. While the surface albedo feedback is often referred to as the explanation of the enhanced Arctic warming, the importance of atmospheric heat transport from the lower latitudes has also been reported in previous studies. In the current study, an attempt is made to understand how the regional feedbacks in the Arctic are induced by the change in atmospheric heat transport and vice versa. Equilibrium sensitivity experiments that enable us to separate the contributions of the Northern Hemisphere mid-high latitude response to the CO₂ increase and the remote influence of surface warming in other regions are carried out. The result shows that the effect of remote forcing is predominant in the Arctic warming. The dry-static energy transport to the Arctic is reduced once the Arctic surface warms in response to the local or remote forcing. The feedback analysis based on the energy budget reveals that the increased moisture transport from lower latitudes, on the other hand, warms the Arctic in winter more effectively not only via latent heat release

but also via greenhouse effect of water vapor and clouds. The change in total atmospheric heat transport determined as a result of counteracting dry-static and latent heat components, therefore, is not a reliable measure for the net effect of atmospheric dynamics on the Arctic warming. The current numerical experiments support a recent interpretation based on the regression analysis: the concurrent reduction in the atmospheric poleward heat transport and future Arctic warming predicted in some models does not imply a minor role of the atmospheric dynamics. Despite the similar magnitude of poleward heat transport change, the Arctic warms more than the Southern Ocean even in the equilibrium response without ocean dynamics. It is shown that a large negative shortwave cloud feedback over the Southern Ocean, greatly influenced by low-latitude surface warming, is responsible for this asymmetric polar warming.

1 Introduction

It is well known that the Arctic experiences larger warming than the rest of the world under the elevated atmospheric CO₂ concentration. In this so-called Arctic amplification, ice albedo feedback plays a central role (Laîné et al. 2016; Yoshimori et al. 2014b). While the ice albedo feedback is a process operating mainly in the polar regions, the magnitude of Arctic warming is well correlated to the global mean warming among climate models. Figure 1 shows the relation between global and Arctic ($\geq 70^\circ\text{N}$) mean surface air temperature changes during the twenty-first century for Coupled Model Intercomparison Project 5 (CMIP5) models, and high correlations exist in two scenarios of Representative Concentration Pathways (RCP) 4.5 and 8.5 (Taylor et al. 2012). Because the surface area of the Arctic region is relatively small, the globally averaged surface air

✉ Masakazu Yoshimori
myoshimo@ees.hokudai.ac.jp

¹ Faculty of Environmental Earth Science, Global Institution for Collaborative Research and Education, and Arctic Research Center, Hokkaido University, Kita 10, Nishi 5, Kita-ku, Sapporo 060-0810, Japan

² Atmosphere and Ocean Research Institute, The University of Tokyo, Kashiwa, Japan

³ National Institute of Polar Research, Tokyo, Japan

⁴ Japan Agency for Marine-Earth Science and Technology, Yokohama, Japan

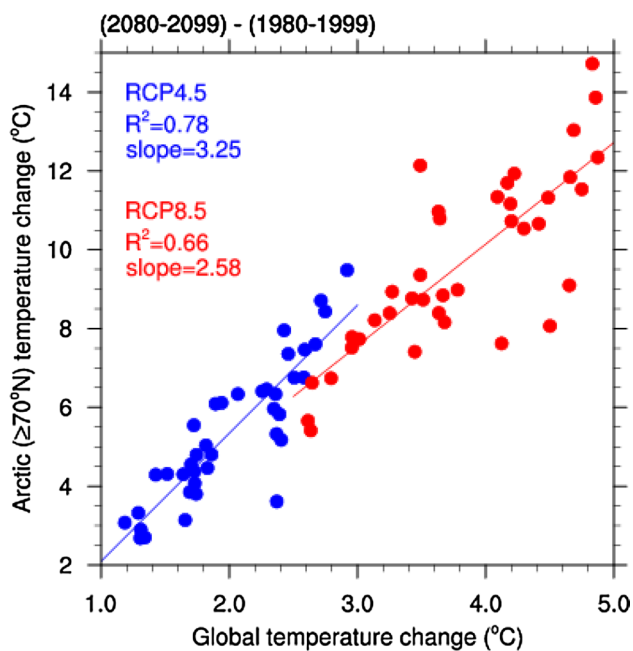


Fig. 1 Relation between global and Arctic temperature changes during the twenty-first century in the RCP4.5 (blue) and RCP8.5 (red) scenarios for 40 CMIP5 models. R^2 indicates variance shared by the two variables while the slope corresponds to that of linear regressions. CMIP5 models (run number r1i1p1) are ACCESS1-0, ACCESS1-3, BCC-CSM1-1, BCC-CSM1-1(m), BNU-ESM, CCSM4, CESM1-BGC, CESM1-CAM5-1-FV2, CESM1-CAM5, CMCC-CMS, CMCC-CM, CNRM-CM5, CSIRO-Mk3-6-0, CanESM2, EC-EARTH, FGOALS-g2, FGOALS-s2, FIO-ESM, GFDL-CM3, GFDL-ESM2G, GFDL-ESM2M, GISS-E2-H-CC, GISS-E2-H, GISS-E2-R-CC, GISS-E2-R, HadGEM2-AO, HadGEM2-CC, HadGEM2-ES, INM-CM4.0, IPSL-CM5A-LR, IPSL-CM5A-MR, IPSL-CM5B-LR, MIROC-ESM-CHEM, MIROC-ESM, MIROC5, MPI-ESM-LR, MPI-ESM-MR, MRI-CGCM3, NorESM1-ME, and NorESM1-M

temperature change is only about 5–7% larger than the spatially averaged value excluding the Arctic region (8–11% if the Arctic is defined as the region $\geq 60^\circ\text{N}$). While these data do not exclude a possibility of Arctic indirectly warming other regions, it is likely that there is a strong thermal influence on the Arctic region from the rest of the world.

The importance of atmospheric heat transport in the Arctic warming is reported in many previous studies. Cai (2005) used a 4-box conceptual model to propose a dynamical amplification mechanism in which the increased poleward atmospheric heat transport leads to Arctic amplification that is further enhanced by water vapor feedback in the warmer Arctic. Lu and Cai (2010) used an idealized atmospheric general circulation model (AGCM) with no seasonal cycle to show that the Arctic amplification can occur even without strong evaporative cooling at low latitudes, positive ice albedo feedback at high latitudes, nor an increase in poleward atmospheric transport of latent heat (LH). In their particular

experimental setting, the amplified warming is attributed to the increase in poleward atmospheric transport of dry-static energy (DSE). Solomon (2006) argued for the importance of LH transport in future Arctic warming by extrapolating a strong relation between LH release in extratropical storms and poleward heat transport by transient eddies in the current climate. Graversen et al. (2008) found a prominent influence of increased atmospheric poleward heat transport on the Arctic warming in a particular reanalysis dataset, but the robustness of the dataset was questioned by subsequent studies (Alexeev et al. 2012; Bitz and Fu 2008; Grant et al. 2008; Screen and Simmonds 2011; Thorne 2008).

The role of atmospheric heat transport in the Arctic warming is also investigated by applying latitude-dependent forcing to numerical models. Alexeev et al. (2005) conducted experiments by adding a heat flux anomaly to the tropical and extra-tropical regions, separately, using two aqua-planet AGCMs coupled to a slab ocean model without seasonal cycle and ice albedo feedback. They showed that a significant Arctic warming occurs even under tropical-only forcing although the pronounced Arctic amplification occurs under extra-tropical forcing. In addition, they demonstrated with an energy balance model that the Arctic amplification occurs when the poleward heat transport is parameterized such that the transport increases with the global mean temperature rise (associating with LH transport) and not with the meridional temperature gradient (associating with DSE transport). Chung and Räisänen (2011) conducted sensitivity experiments using two AGCMs coupled to slab ocean models under CO_2 forcing that depends on latitudes: one only in the Northern Hemisphere (NH) high latitudes and the other only in other regions. They found that the most profound Arctic surface warming is simulated when the model is forced with the remote CO_2 forcing, and attributed the warming to the increased poleward atmospheric heat transport. The details of the mechanisms are, however, not presented. Screen et al. (2012) investigated the relative role of observed changes in sea surface temperature (SST) and sea ice distribution with two AGCMs by prescribing them globally or only in the Arctic region. Their results show that near-surface warming in autumn to winter is primarily caused by the Arctic sea surface changes while warming above 700 hPa in the same season is mainly caused by the change in remote sea surface conditions. While their study clearly isolated the effect of atmospheric dynamics on the Arctic warming, the prescribed sea surface conditions did not reveal how the atmospheric dynamics interacts with other climate feedback processes. We note that Chung and Räisänen (2011) and the current study suggest that a large part of the prescribed Arctic sea surface changes in Screen et al. (2012) are forced remotely.

Hwang et al. (2011) found a negative (positive) correlation between the Arctic amplification and the poleward atmospheric (ocean) heat transport change over the twenty-first century among 10 CMIP3 models. They also showed that poleward LH transport increases while DSE transport decreases at NH high latitudes for all of the models, while the sign of moist static energy ($MSE = DSE + LH$) transport change depends on the model. Recently, Graverson and Burtu (2016) applied a regression analysis to the daily-scale variations of meridional heat transport of the atmosphere and Arctic temperature, clouds, and radiation. They scaled the regression relation to the change between the twentieth and twenty-first centuries and concluded that the contribution of the LH transport increase is about one order of magnitude larger than the contribution of the same amount of DSE transport increase. In their analysis, however, the seasonal dependence was not taken into account.

In summary, it is still unclear how the atmospheric heat transport interacts with other regional feedbacks in the Arctic and leads to the Arctic warming under a realistic model configuration (seasonal cycle and geography). In the present study, we investigate the role of atmospheric heat transport and its interactions with regional feedbacks in the Arctic without considering the ocean dynamical feedback. We note, however, that the importance of ocean heat transport was pointed out in other studies (Holland and Bitz 2003; Mahlstein and Knutti 2011). The uniqueness of our approach is that sensitivity experiments, in which forcing is essentially partitioned into NH mid-high latitudes and other regions, and detailed feedback analysis based on the energy budget analysis are combined. By so doing, we are able to quantify the role of remote and local forcing and their association with various feedbacks involved.

The paper is organized as follows. In the next section, the models and experiments are described. The analysis method is explained in Sect. 3. Section 4 presents the results followed by discussions and conclusions given in Sects. 5 and 6, respectively.

2 Model and experiments

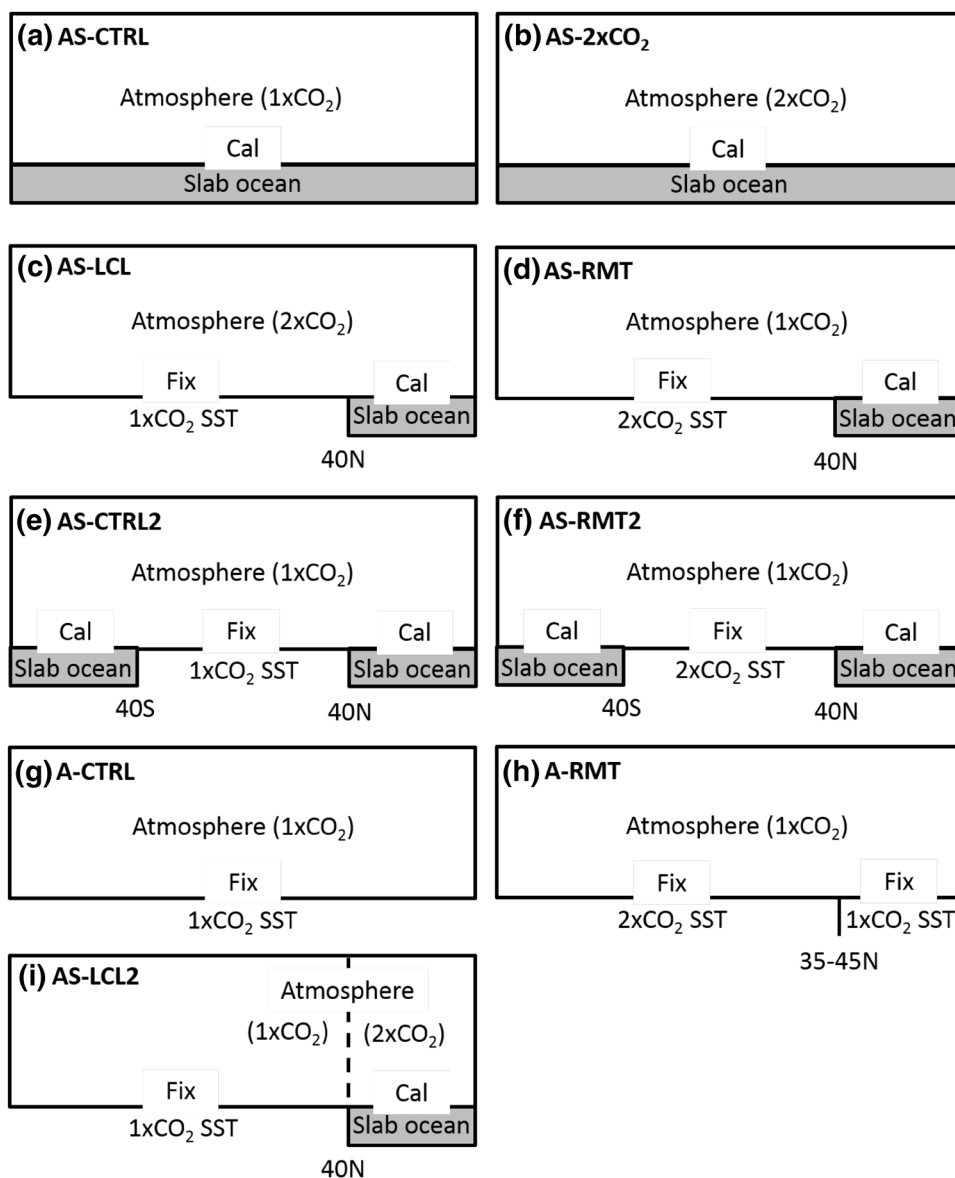
The model used in the present study is an atmospheric general circulation model (GCM) coupled to a mixed-layer slab ocean model, and is identical to that used in Yoshimori et al. (2014b). We note that the atmospheric model component is identical to that of the coupled atmosphere–ocean GCM, MIROC4m used in Yoshimori et al. (2014a), and a suite of experiments with essentially the same model as MIROC4m were archived in the CMIP3 (Meehl et al. 2007). The ocean model component has a constant depth of 50 m and solves only the thermodynamic equation and does not calculate the circulation. Therefore, the effect of

the ocean heat transport is represented by an additional heat flux (so-called Q-flux) term which is determined to reproduce the observed seasonal march of SST and sea ice distribution under present-day conditions. Q-flux varies monthly and from place to place, but not between the experiments. All model components, atmosphere, land, ocean, and sea ice, share the same horizontal resolution of T42 ($\sim 2.8^\circ$) and the atmosphere has 20 vertical levels.

Experiments conducted in the present study are illustrated in Fig. 2 and described here in details. All experiments are conducted to investigate the equilibrium response. The AS-CTRL experiment is run under the pre-industrial conditions, and serves as a control experiment (Fig. 2a). The AS-2xCO₂ experiment is the same as AS-CTRL except that the atmospheric CO₂ concentration is doubled (Fig. 2b). In AS-CTRL and AS-2xCO₂, both SST and sea ice mass at every grid points are computed in the model (sea ice concentration is diagnosed from the mass). The AS-LCL experiment in Fig. 2c is the same as AS-2xCO₂ except that SST and sea ice mass to the south of 40°N are prescribed by those in AS-CTRL. The AS-RMT experiment in Fig. 2d is the same as AS-CTRL except that SST and sea ice mass to the south of 40°N are prescribed by those in AS-2xCO₂. In comparison with AS-CTRL, AS-LCL is aimed to isolate the response of the Northern Hemisphere (NH) mid-high latitude surface warming to the CO₂ radiative forcing. It does, however, include the effect of land surface response to the elevated CO₂ concentration at other latitudes. Thus, a supplementary experiment with only NH mid-high latitude CO₂ forcing (Fig. 2i with linearly increasing CO₂ from 1xCO₂ to 2xCO₂ in 35–45°N) is conducted to see the effect of land surface warming in remote latitudes on the Arctic warming. In comparison with AS-CTRL, AS-RMT is aimed to isolate the effect of remote surface warming on the NH mid-high latitude response. The boundary latitude of 40°N is located south of the maximum seasonal extent of NH sea ice cover, and this choice guarantees not to introduce any artificial discontinuities in sea ice distribution in the two sensitivity experiments (AS-LCL and AS-RMT).

Two other experiments are conducted to investigate the reason for the asymmetric polar warming of Northern and Southern hemispheres by using the slab ocean model in mid and high latitudes of both hemispheres (AS-CTRL2 and AS-RMT2 as in Fig. 2e, f). In both experiments, the oceans north of 40°N and south of 40°S are represented by the slab ocean model while the SST was prescribed between 40°S and 40°N. Atmospheric CO₂ concentration was fixed at the 1xCO₂ level. In the first experiment (AS-CTRL2), the prescribed 40°S–40°N SST was taken from the AS-CTRL and it was replaced by the SST from AS-2xCO₂ in the second experiment (AS-RMT2). AS-CTRL, AS-2xCO₂, AS-LCL, AS-RMT, AS-CTRL2, and AS-RMT2 experiments are

Fig. 2 Illustration of the experiments. “Fix” and “Cal” stand for fixed and calculated lower boundary conditions of the atmosphere (i.e., SST and sea ice conditions), respectively. See text for the details of each experiment



integrated for 60 years, and the last 30 years are used for the analysis.

The slab ocean model component is removed from the last two experiments, A-CTRL and A-RMT as in Fig. 2g, h, respectively, and the model is simply an atmospheric GCM. In A-CTRL, SST and sea ice mass are prescribed by those in the AS-CTRL while they are combined from AS-CTRL and AS- $2xCO_2$ in A-RMT. The pre-industrial atmospheric CO_2 concentration is prescribed in both experiments. A-CTRL may be replaced by the AS-CTRL, but it is nevertheless conducted for completeness, and the result of A-RMT is always referenced to that of A-CTRL. In the A-RMT, SST and sea ice mass from AS-CTRL are prescribed to the north of $45^\circ N$ while those from the AS- $2xCO_2$ are prescribed to the south of $35^\circ N$. In between,

they are linearly interpolated in order to avoid the artificial jump of the prescribed boundary conditions. In comparison with A-CTRL, A-RMT is aimed to isolate the effect of remote surface warming via atmospheric dynamics by essentially disabling the NH mid-high latitude surface warming. We note, however, that the surface temperature on snow and sea ice is allowed to change in A-RMT with respect to A-CTRL even though sea ice mass is fixed. A-CTRL and A-RMT experiments are integrated for 40 years, and the last 30 years are used for the analysis.

Our experimental design is aimed to answer questions on how large the NH mid-high latitude response alone to CO_2 radiative forcing is and how that is magnified if the surface warming feedback outside of the region is added.

3 Analysis method

3.1 Atmospheric energy transport

The zonal mean, northward atmospheric energy transport at a pressure level may be decomposed into three components of mean meridional circulation, stationary eddies, and transient eddies:

$$[\overline{hv}] = [\overline{h}] [\overline{v}] + [\overline{h^*} \overline{v^*}] + [\overline{h'v'}] \tag{1}$$

where square bracket and overbar denote zonal and time averages, respectively, and star and dash denote the deviations from the zonal and time averages, respectively. Here, v is northward wind velocity, and

$$h \equiv c_p T + \phi + Lq \tag{2}$$

is the moist static energy with T air temperature, ϕ geopotential, q specific humidity, c_p specific heat at constant pressure, and L latent heat of vaporization. Kinetic energy is ignored in the present study. Keith (1995) presented a formula equivalent to (1) for more generalized vertical coordinate:

$$[\overline{hva}] = \frac{[\overline{h\alpha}] [\overline{v\alpha}]}{[\overline{\alpha}]} + \left[\left(\overline{h} - \frac{[\overline{h\alpha}]}{[\overline{\alpha}]} \right) \left(\overline{v} - \frac{[\overline{v\alpha}]}{[\overline{\alpha}]} \right) \overline{\alpha} \right] + \left[\left(h - \frac{\overline{h\alpha}}{\overline{\alpha}} \right) \left(v - \frac{\overline{v\alpha}}{\overline{\alpha}} \right) \alpha \right] \tag{3}$$

where α denotes a layer thickness of the atmospheric level of interest. In the model used here, the vertical coordinate is defined by specifying $\sigma \equiv p/p_s$, i.e., pressure p normalized by the surface pressure p_s . Thus, $\alpha = \Delta p = p_s \Delta \sigma$ in our case. The second and triple moments are computed at every time step during the model integration and their monthly mean values are stored as model output. Therefore, our time average represents monthly mean, and the transient eddy represents sub-monthly variabilities.

$$\Delta \mathbf{R} \equiv \Delta \mathbf{R}_{SW}^{EXT} + \Delta \mathbf{R}_{SW}^{WVP} + \Delta \mathbf{R}_{SW}^{ALB} + \Delta \mathbf{R}_{SW}^{CLD} + \Delta \mathbf{R}_{SW}^{ERR} + \Delta \mathbf{R}_{LW}^{EXT} + \Delta \mathbf{R}_{LW}^{WVP} + \Delta \mathbf{R}_{LW}^{CLD}, \tag{5}$$

$$\Delta \mathbf{Q} \equiv \Delta \mathbf{Q}^{EVP} + \Delta \mathbf{Q}^{SH} + \Delta \mathbf{Q}^{LSC} + \Delta \mathbf{Q}^{CUM} + \Delta \mathbf{Q}^{VDF} + \Delta \mathbf{Q}^{DYN} + \Delta \mathbf{Q}^{RES} \tag{6}$$

3.2 Climate feedback–response analysis method

In order to decompose the simulated temperature change to contributions of individual processes, we adopt the climate feedback-response analysis method (CFRAM) originally developed by Lu and Cai (2009a) and applied in many studies including those on the Arctic warming amplification (Cai and Lu 2009; Sejas et al. 2014; Taylor et al. 2013; Yoshimori et al. 2014a, b). The CFRAM solves the energy

budget equations at all layers of the atmosphere and the surface simultaneously, and a three dimensional composition is thus obtained. This approach has an advantage compared to solving the energy balance equation at the surface (Laîné et al. 2016) or at the top of the atmosphere (single level diagnosis). In the single level diagnosis, the contribution of temperature anomaly in other layers of the atmosphere to the level of interest is not attributed to physically insightful processes: a part of the surface temperature rise is attributed to the air temperature rise in the layer right above the surface, and a part of the air temperature rise is attributed to the surface temperature rise.

The perturbed energy budget equation for each column of the atmosphere and the surface is given by

$$\Delta \mathbf{T} = \left(\frac{\partial \mathbf{R}_{LW}}{\partial \mathbf{T}} \right)^{-1} (\Delta \mathbf{R} + \Delta \mathbf{Q}) \tag{4}$$

where the perturbation is denoted by Δ , and $\mathbf{T} = (T_1, T_2, \dots, T_N, T_S)^t$ is a transposed vector of temperature at N atmospheric levels and at the surface (T_S). \mathbf{R} and \mathbf{Q} are vectors of $N + 1$ elements which respectively represent radiative and non-radiative components of the energy

flux convergence at every level of the column. $\partial \mathbf{R}_{LW} / \partial \mathbf{T}$ is a Planck response matrix of $(N + 1) \times (N + 1)$ elements which are the divergence of longwave radiative fluxes at $N + 1$ levels due to a unit temperature increase at $N + 1$ levels. The Planck response matrix is precomputed using the radiative transfer part of the atmospheric GCM, and it is identical to that used in Yoshimori et al. (2014a).

Radiative and non-radiative terms are further decomposed into

with SW and LW denoting shortwave and longwave radiation, respectively. The meaning of superscripts in Eqs. (5) and (6) are listed in Table 1. They are identical to the decomposition used in Yoshimori et al. (2014a) except that there is an additional term $\Delta \mathbf{R}_{SW}^{ERR}$, which represents the residual term arising from the estimate of SW radiative fluxes. As stated in Yoshimori et al. (2014a), the error emerges in summer Arctic when the insolation is extremely large. The surface albedo component is diagnosed using

Table 1 A list of acronyms for partial temperature change terms diagnosed with the CFRAM technique (modified from Table 2 of Yoshimori et al. 2014a)

Category	Vector	Abbreviation	Description
Radiative	A+S	EXT	External forcing
	A+S	WVP	Water vapor
	A+S	ALB	Surface albedo
	A+S	CLD	Clouds
	A+S	ERR	Residual in SW diagnostics
Non-radiative	A	LSC	Large-scale condensation
	A	CUM	Cumulus convection
	A	VDF	Boundary layer process
	A	DYN	Advection
	A	DAD	Dry adjustments
	A	RESA	Atmospheric heat storage
	S	EVP	Surface evaporation
	S	SH	Surface sensible heat flux
	S	RESS	Net surface energy flux (ocean heat storage + ocean dynamics + sea ice change)
	A+S	RES	DAD+RESA+RESS

“A” and “S” in the second left column denote non-zero component in the vector \mathbf{R} and \mathbf{Q} in Eq. (4) at atmospheric and surface levels, respectively

the radiative kernel technique in which the precomputed anomalous radiative flux pattern caused by a constant albedo change is scaled by simulated albedo changes. The cloud component is computed by adjusting the difference between total-sky (*ttl*) and clear-sky (*clr*) radiative fluxes with the so-called cloud masking effect:

$$\Delta \mathbf{R}^{CLD} = \Delta \mathbf{R}^{ttl} - \Delta \mathbf{R}^{clr} - \sum_j (\Delta \mathbf{R}^{j,ttl} - \Delta \mathbf{R}^{j,clr}) \quad (7)$$

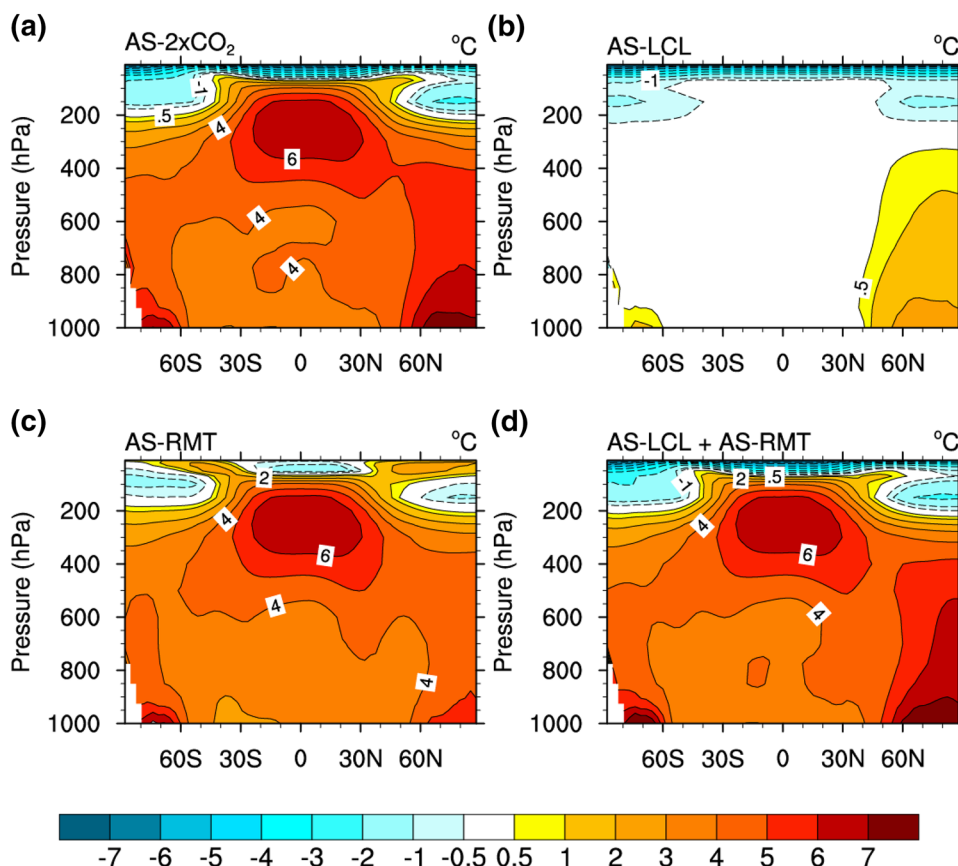
where j represents external forcing, water vapor, surface albedo, and temperature. The procedure is essentially the same as Soden et al. (2008) except that the kernels are applied to compute the radiative fluxes at all levels, rather than only at the top of the atmosphere. We compute $\Delta \mathbf{R}_{SW}^{ERR}$ by subtracting the sum of individually diagnosed SW radiative fluxes with the radiative kernels from the total SW radiative fluxes stored as a model output. We note that atmospheric and surface temperatures are used only to compute the LW cloud masking, and that only the difference between total-sky and clear-sky components is used. We therefore consider that the diagnosed individual CFRAM terms are virtually independent of the simulated temperature change, and that a comparison of the sum of all CFRAM terms with simulated temperature change may be used to evaluate the consistency of the analysis method. In this article, we only present the result of partial surface temperature changes (ΔT_s) by individual terms as in Sejas et al. (2014) although the full equation of (4) including partial air temperature changes is solved.

4 Result

Figure 3 shows the zonal and annual mean atmospheric temperature change from the control simulation. In the CO₂ doubling experiment with the global slab ocean model, well-known features of enhanced warming near the Arctic surface and tropical upper troposphere are simulated (Fig. 3a). We note that the warming is also enhanced near the surface at the Southern Hemisphere (SH) high latitudes, though, to a lesser degree compared to the NH counterpart. The NH mid-high latitudes show, on the other hand, a limited warming in response to the CO₂ forcing when the sea surface in other latitudes are fixed at 1xCO₂ conditions (Fig. 3b). We note that Fig. 3b also includes the effect of global land surface response to the CO₂ forcing, but the result (AS-LCL2) changes little even if the CO₂ forcing is applied only to the NH mid-high latitudes (not shown). Much of the full response seen in the global slab ocean model experiment (Fig. 3a) is captured by the experiment forced by the remote surface warming (Fig. 3c). The addition of warming in the two experiments isolating the remote and local effect (Fig. 3b, c) reproduces the full response reasonably well although small differences are discernible (Fig. 3a, d). This linearity suggests that the comparison of the two sensitivity experiments (AS-LCL and AS-RMT) is meaningful in the context of sensitivity measurement of local and remote influence.

Figure 4a shows the seasonality of surface air temperature change from the control simulation averaged over the

Fig. 3 Zonal and annual mean air temperature changes in the atmosphere from the control experiments (°C): **a** AS-2xCO₂; **b** AS-LCL; **c** AS-RMT; and **d** the sum of the changes in AS-LCL and AS-RMT



Arctic region (north of 70°N). All experiments exhibit least warming in summer (June–July–August). The maximum warming occurs in November except for the experiment with sea surface conditions fixed at the NH mid-high latitudes (A-RMT). In A-RMT, the warming occurs unsurprisingly by a similar magnitude throughout the year. The sea ice distribution exhibits common seasonal features of both minimum extent and maximum reduction in September as long as the sea ice is allowed to respond to the forcing (Fig. 4b). Figure 4c shows the seasonal evolution of ocean mixed-layer temperature (or SST) change from the control simulation averaged over the Arctic region. It exhibits the maximum warming in September when sea ice reduction is also maximum. The magnitude of the SST change is small as the heat capacity of the ocean is large and the SST is fixed at the melting point when the ocean is covered by ice (cf. Fig. 5). The important point is that the maximum of ocean heat content anomaly occurs earlier than the maximum of surface air temperature anomaly. Surface temperature anomaly is large during late autumn to early winter because the warm sea surface is more exposed to the atmosphere where the ice is removed and because the anomalous oceanic heat stored in summer is released vigorously to the much colder atmosphere. The released heat warms the near-surface atmosphere (and ice-covered

surface) efficiently in winter when near-surface atmospheric stratification is large.

Figure 5 shows the sea ice distribution in September when the monthly reduction is the largest. Consistent with Fig. 3, the reduction of sea ice concentration is larger in the experiment with remote forcing (Fig. 5d) than that with CO₂ forcing (Fig. 5c). Here the nonlinearity is obvious, that is the addition of sea ice changes in AS-LCL and AS-RMT (Fig. 5c–a, d–a) does not reproduce the full response of AS-2xCO₂ (Fig. 5b–a) because the sea ice melting starts from the southern edges in each isolated-forcing experiment. Nevertheless, it is still useful to compare the response to perturbations from the same reference climate (i.e., control simulation).

As the ocean dynamics is suppressed in the slab ocean model, any remote influence must come via atmospheric dynamics. Figure 6a–c show the changes in the northward atmospheric transport of moist static energy (MSE), latent heat (LH), and dry static energy (DSE) from the control simulation, respectively. In A-RMT, in which sea surface warming is essentially suppressed in the regions north of 40°N and sea surface warming is prescribed in other latitudes, the poleward MSE transport increases by 18% near 40°N. Once the SST and ice are allowed to respond in the regions north of 40°N (AS-RMT), the poleward

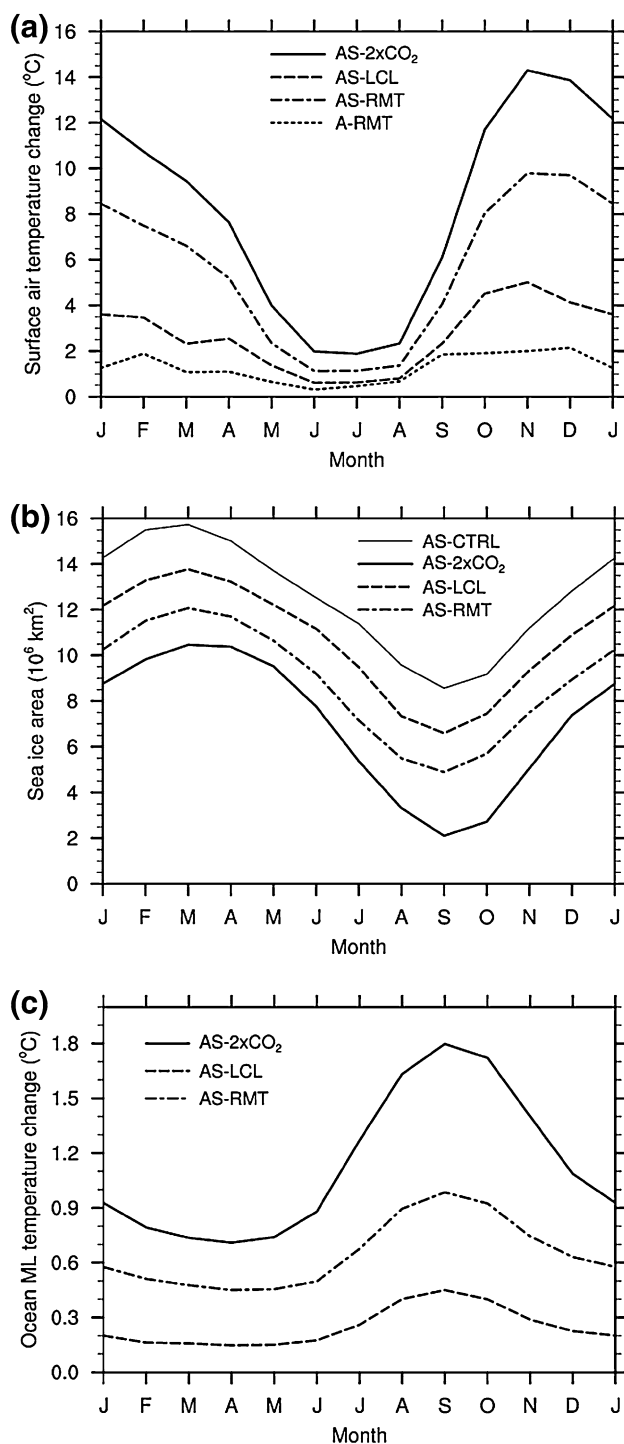


Fig. 4 Annual cycle: **a** change in surface air temperature ($^\circ\text{C}$) in the Arctic region ($\geq 70^\circ\text{N}$) from the control experiments; **b** sea ice area ($\times 10^6 \text{ km}^2$) in the Northern Hemisphere; and **c** change in ocean mixed-layer temperature ($^\circ\text{C}$) in the Arctic region ($\geq 70^\circ\text{N}$) from the control experiment

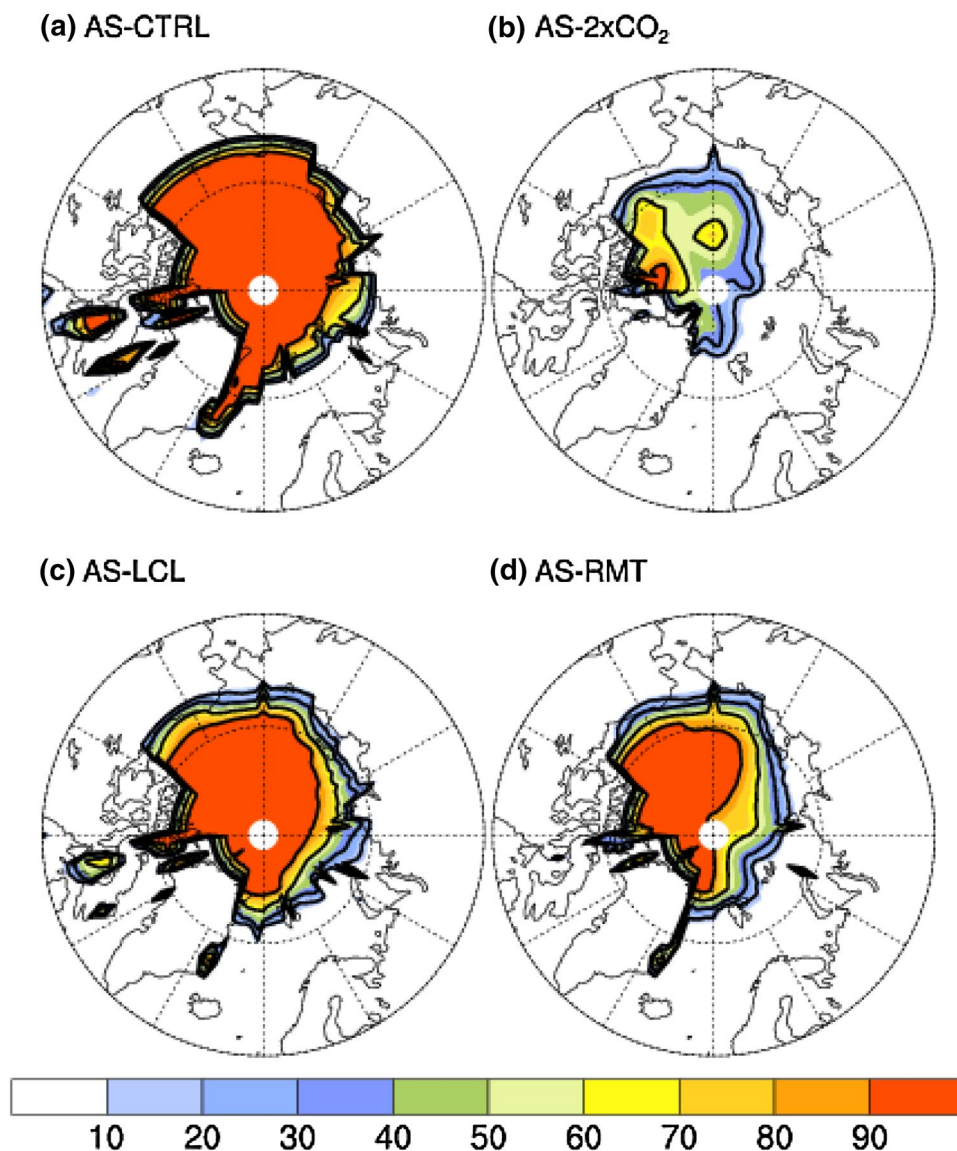
MSE transport decreases significantly near 40°N relative to A-RMT. This occurs mainly through a reduction in the DSE component, and to a lesser extent in the LH

component. Consistently, the warming in the regions north of 40°N leads to a reduction of northward DSE and MSE transport in AS-LCL relative to AS-CTRL. As a result of counteracting contributions of increased LH and decreased DSE transport, the poleward MSE transport increases in the regions north of 40°N for the AS-2xCO₂. In summary, the net effect of the remote surface warming on the poleward atmospheric heat transport is an increase of the LH component while the net effect of local response to CO₂ forcing is a decrease of poleward DSE. These results may not be surprising as the low-latitude warming increases atmospheric moisture content to be transported and the high-latitude warming reduces atmospheric meridional temperature gradient. The concurrent reduction in the meridional surface temperature gradient and increase in the DSE transport in the dry model of Lu and Cai (2010), however, suggests that the meridional near-surface temperature gradient may not be responsible for the DSE transport change. The concurrent increase in the meridional upper-tropospheric temperature gradient and decrease in the DSE transport in AS-2xCO₂, on the other hand, suggests that the meridional upper tropospheric temperature gradient is not a determinant factor either. While it is still possible that the DSE transport change process is different between dry and moist models, it remains to be investigated what determines the partition of DSE and LH components in the total atmospheric heat transport change.

Atmospheric latent heat transport to the Arctic region through the 70°N circle is shown in Fig. 7. Throughout the year, poleward LH transport increases in all experiments although there are months that exhibit neutral changes in AS-LCL. A comparison of total LH transport change (Fig. 7a) and that due to transient eddy component (Fig. 7b) indicates that much of the change is accomplished by sub-monthly transient eddies. We note that the increase in AS-LCL is fairly small compared to other experiments even though the surface warms between 40°N and 70°N . This result indicates that low-latitude warming is a key to increase the atmospheric latent and hence total heat transport to the Arctic region.

Figure 8 shows the partial surface temperature change with respect to the control simulation averaged over the Arctic region for individual months diagnosed using the CFRAM technique. To ease readability, only albedo feedback (ALB) and surface heat uptake (RESS) terms are explicitly displayed here with the rest terms shown collectively, the ‘Others’ term. The simulated change (SIM) is well reproduced by the sum of all terms diagnosed by the CFRAM technique (SUM). In AS-2xCO₂, AS-LCL, and AS-RMT, the albedo feedback which tends to warm the surface in summer is nearly cancelled by the surface heat uptake that represents the energy consumed for ocean warming and sea ice melting. At the zeroth order, the

Fig. 5 Sea ice concentrations in September (%): **a** AS-CTRL; **b** AS-2xCO₂; **c** AS-LCL; and **d** AS-RMT. Contours indicate 15, 30, 60, and 90% concentrations



seasonal evolution of the Arctic surface warming is characterized by the absorption of heat anomaly in summer and its release in winter, consistent with previous studies (Lu and Cai 2009b; Yoshimori et al. 2014a). There are other terms that significantly contribute to winter warming in the AS-RMT, however. In A-RMT, the term 'Others' has a dominant potential for the surface warming, which is suppressed by the surface heat uptake due to the prescribed sea surface conditions with infinite heat capacity. We note that the increase of surface albedo is seen in spring through an increase of snow amount on sea ice, probably due to an increased precipitation.

In order to investigate how the other feedbacks may be important, 'Others' term in Fig. 8 is presented individually in Fig. 9 for A-RMT and AS-RMT. A-RMT reveals how the atmospheric dynamics induced by the remote surface warming tends to warm the Arctic surface while the

difference of the two experiments reveals how the NH mid-high latitude surface response feeds back to the Arctic surface warming. Figure 9a shows that the increased poleward transport of DSE (DYN) and LH (LSC) warms the Arctic atmosphere which in turn tends to warm the surface (LSC includes the local evaporation as a moisture source, but the evaporation is decreased in A-RMT). In addition, the increased water vapor transport tends to warm the Arctic surface through greenhouse effect of water vapor (WVP) and clouds (CLDL). As the evaporation and consequent potential cooling (EVP) is reduced with the increased near-surface air temperature (whereas surface temperature is essentially fixed) (Fig. 9a; cf. Equation (9) of Laine et al. 2014), the moisture source of increased water vapor and clouds most likely originates from remote regions and is transported horizontally via the atmosphere (cf. Fig. 7b). The fractional contribution of water vapor, clouds, and

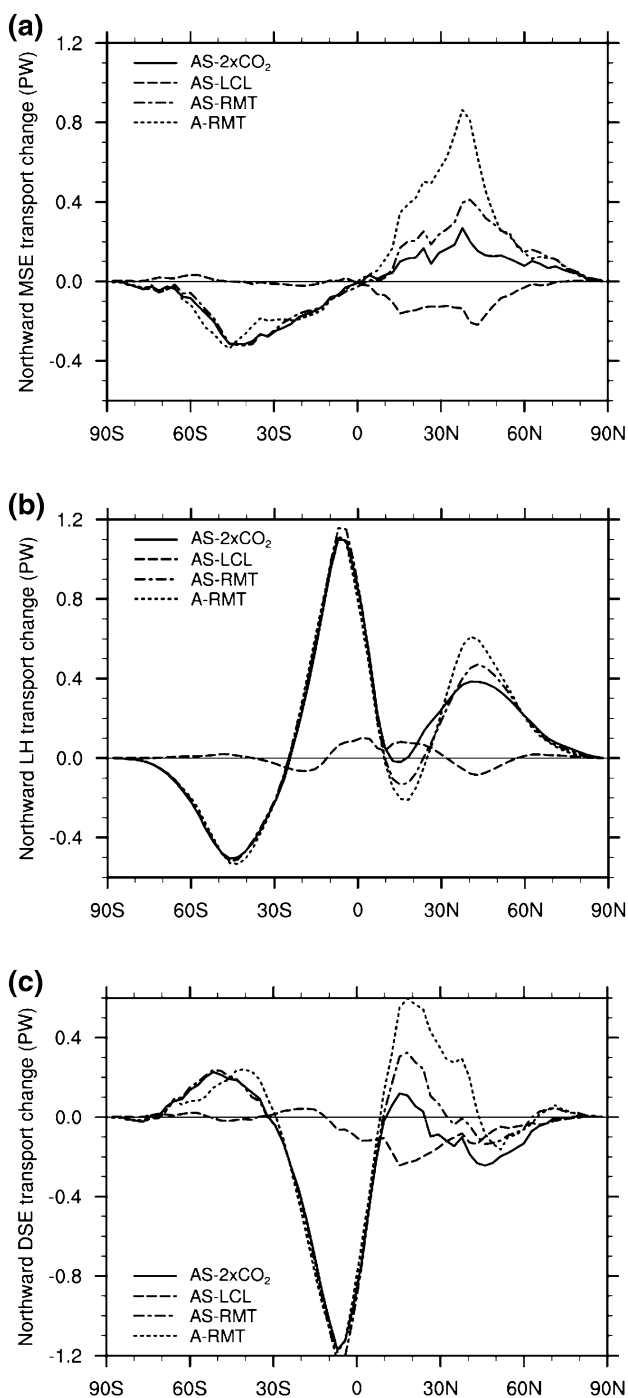


Fig. 6 Annual mean northward energy transport changes in the atmosphere (PW): **a** moist static energy; **b** latent heat; and **c** dry static energy

large-scale condensation to the total Arctic surface temperature change amounts to about 58% while dynamical heating and evaporative cooling contribute 18 and 17%, respectively, on the October–November–December average. As the increase in the northward atmospheric DSE and LH transport at 70°N are about equal, the LH transport appears

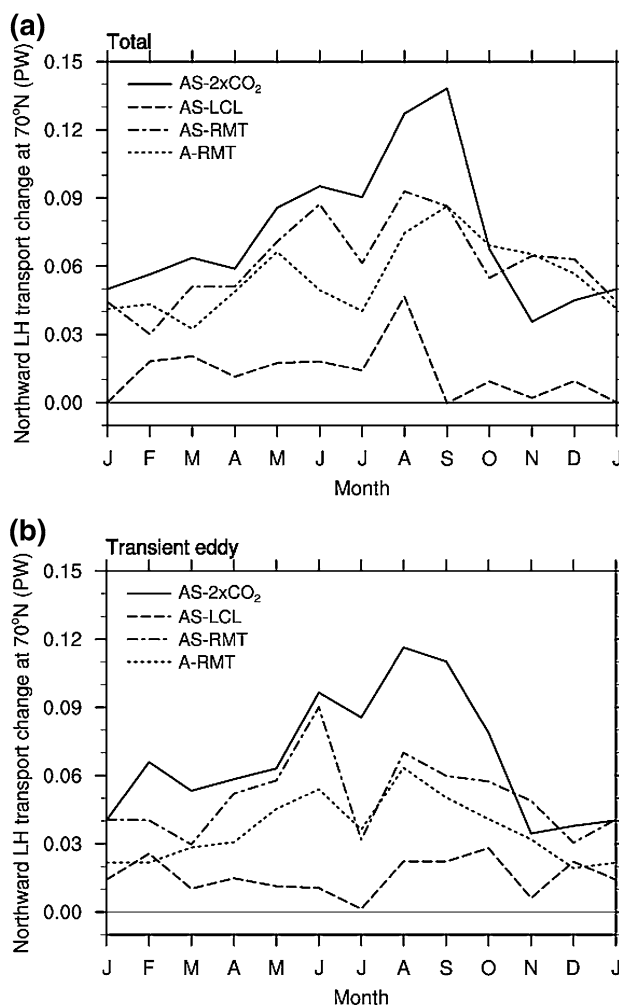


Fig. 7 Annual cycle of the northward latent heat transport at 70°N in the atmosphere (PW): **a** total changes; and **b** changes due to sub-monthly transient eddy

to be much more effective in warming the Arctic surface through the greenhouse effect of water vapor and clouds as also found by Graversen and Burtu (2016).

Once the sea surface is allowed to respond, an enhanced greenhouse effect of clouds is further strengthened and contributes positively to the Arctic surface warming (CLDL in Fig. 9c). At the same time, evaporative and advective coolings are induced and they contribute negatively to the Arctic surface warming (DYN and EVAP in Fig. 9c). Also, the sun-shade effect by clouds becomes substantial in summer (CLDS in Fig. 9b, c). It is verified that the increase of low-level clouds can indeed be induced by remote surface warming without significant Arctic surface warming in autumn (Fig. 10d). In Fig. 10a–c, the increase of low-level clouds is more concentrated in the regions of reduced sea ice cover (Fig. 5). It is shown that lower tropospheric stability increases due to the effect of remote surface warming while the mid-high latitude response tends to reduce the

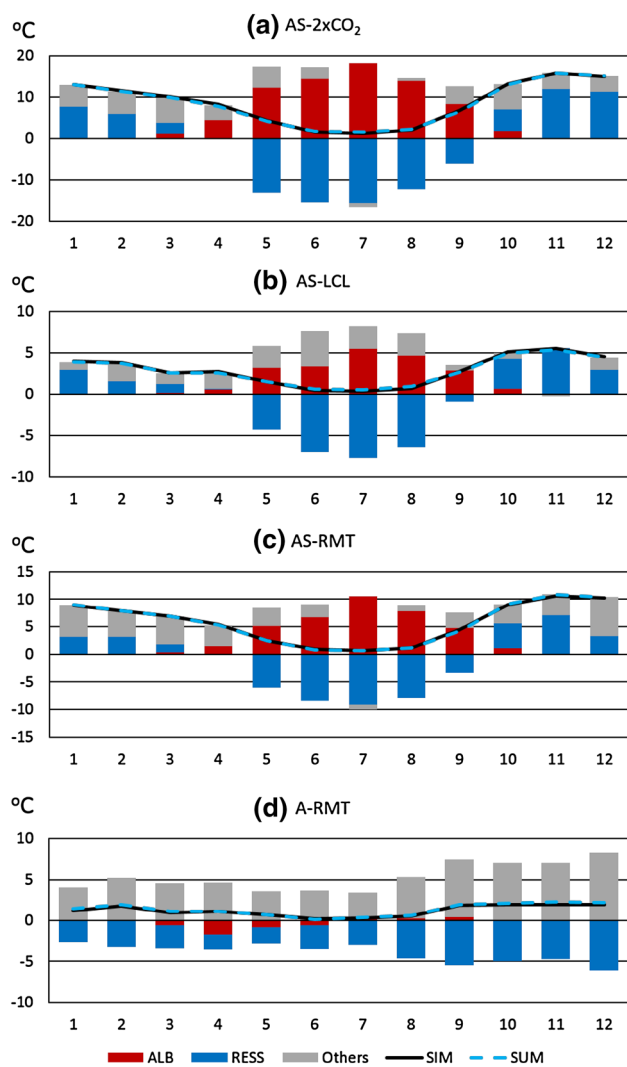


Fig. 8 Monthly partial surface temperature changes with respect to the control experiments diagnosed using the CFRAM technique (°C): **a** AS-2xCO₂; **b** AS-LCL; **c** AS-RMT; and **d** A-RMT. *ALB* albedo feedback, *RESS* snow-ice melting and ocean heat uptake, *OTHERS* other terms, *SUM* sum of all terms of the partial temperature change (*SUM*=*ALB*+*RESS*+*OTHERS*), and *SIM* simulated skin temperature change. The partial temperature change in the vertical axis is averaged to the north of 70°N

stability (Fig. 11a). The vertical structure of Fig. 11b also suggests that the water vapor anomaly is mostly supplied via the atmospheric transport under remote forcing, rather than from the local surface, in A-RMT. We note that the difference in vertical profiles in response to remote and surface forcing are qualitatively similar to Fig. 11 of Alexeev et al. (2005).

Given the approximate symmetry in the increased atmospheric heat transport to the NH and SH high latitudes in AS-2xCO₂ (Fig. 6a, b) and the importance of remote forcing in the Arctic warming, one may wonder why the Southern Ocean does not warm as much as the Arctic Ocean (Fig. 3a).

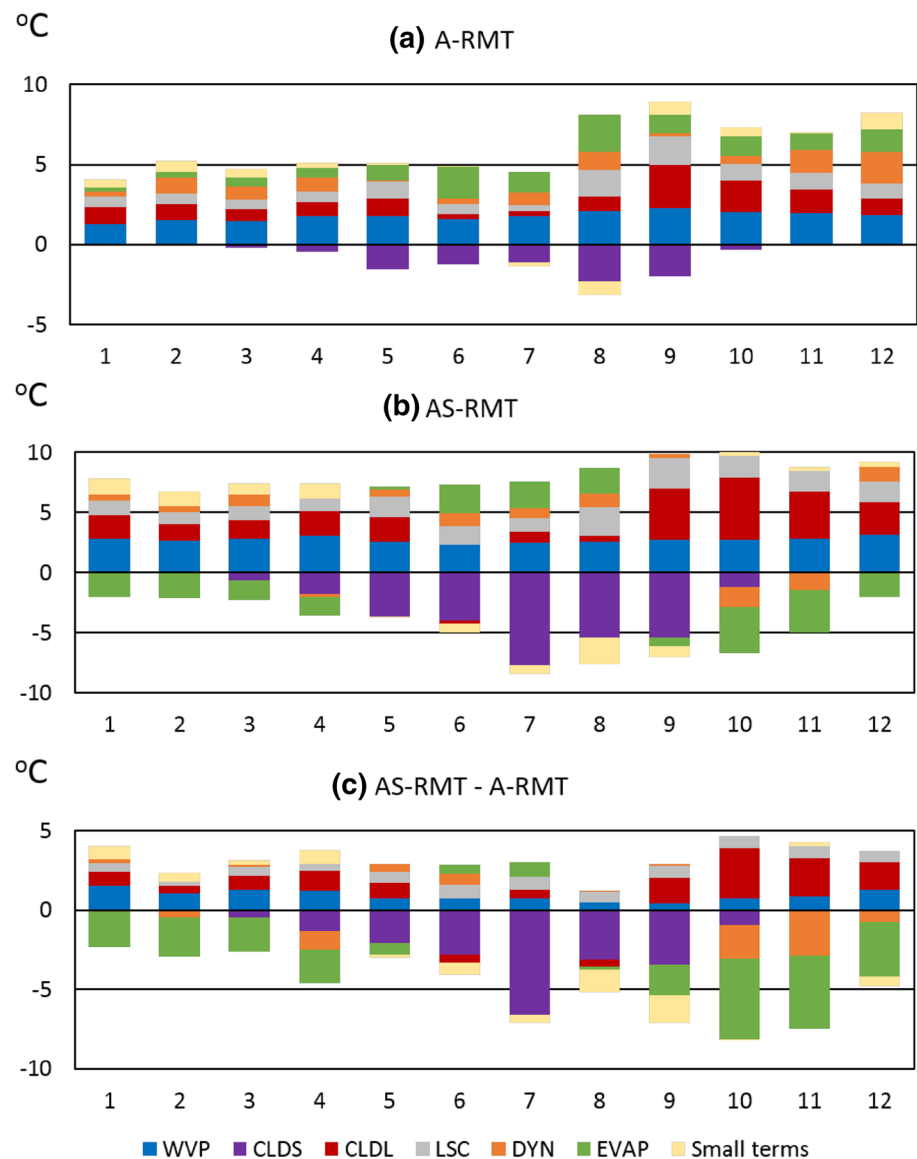
In transient climate simulations using coupled atmosphere–ocean GCMs, larger ocean heat uptake and effective heat capacity in the Southern Ocean (Yoshimori et al. 2016) and changes in ocean circulation (Armour et al. 2016; Marshall et al. 2014) are often cited as reasons for the asymmetric polar warming. For the current equilibrium response without ocean dynamics, an alternative explanation is required. In order to seek the answer to this fundamental question, we conduct two additional experiments (AS-CTRL2 and AS-RMT2). In these experiments, the effect of remote warming in lower latitudes on both polar regions are compared. The black solid line in Fig. 12 represents simulated surface temperature changes and the asymmetric polar warming between AS-RMT2 and AS-CTRL2. Other lines in Fig. 12 represent partial surface temperature changes for selected terms diagnosed using the CFRAM technique. While the albedo, large-scale condensation, and LW cloud terms contribute to the warming roughly at the same magnitude between the Arctic and the Southern Ocean, the SW cloud term exhibits a striking difference between the two regions. The large cooling effect by clouds in the Southern Ocean is explained by an increase in the cloud amount associated with the solid to liquid phase change of cloud condensate and consequent increase in cloud life time under warming, as elaborated by Ogura et al. (2008a, b), and discussed by Yoshimori et al. (2009).

In the NH, the large negative SW cloud feedback occurs in July and August to the north of 70°N. In the lower troposphere, this latitudinal zone approximately coincides with the climatological mixed-phase cloud region of the model (−15 to 0°C). In the same season, the SW cloud feedback is positive to the south of 70°N where the land response dominates and the cloud decreases over the Norwegian Sea. In the SH, the climatological mixed-phase cloud region is located near 60°S in the lower troposphere throughout the year.

The weaker negative SW cloud feedback over the Arctic Ocean compared to the Southern Ocean is understood by the difference in the climatological distribution of cloud condensate. The amount of cloud condensate peaks at about 40°–60° latitudinal band in the lower troposphere of both hemispheres. The feedback associated with the cloud phase change works strongly where the cloud condensate is abundant. Consequently, the stronger negative SW cloud feedback emerges in the Southern Ocean.

We found that the contrast in the SW cloud feedback between the two polar regions in AS-2xCO₂ is grossly captured by the AS-RMT2 with only remote surface warming. Provided that there is a large model spread in the Southern Ocean cloud response to the global warming as explored by Tsushima et al. (2006), the exact level of asymmetry between the Arctic and Southern Ocean warmings in the equilibrium response is likely uncertain.

Fig. 9 Monthly partial surface temperature changes of selected terms ('Others' in Fig. 8) with respect to the control experiment diagnosed using the CFRAM technique (°C): **a** A-RMT; **b** AS-RMT; and **c** the difference between AS-RMT and A-RMT. *WVP* water vapor, *CLDS* shortwave cloud, *CLDL* longwave cloud, *LSC* large-scale condensation, *DYN* advection, and *EVAP* evaporative cooling. The partial temperature change in the vertical axis is averaged to the north of 70°N



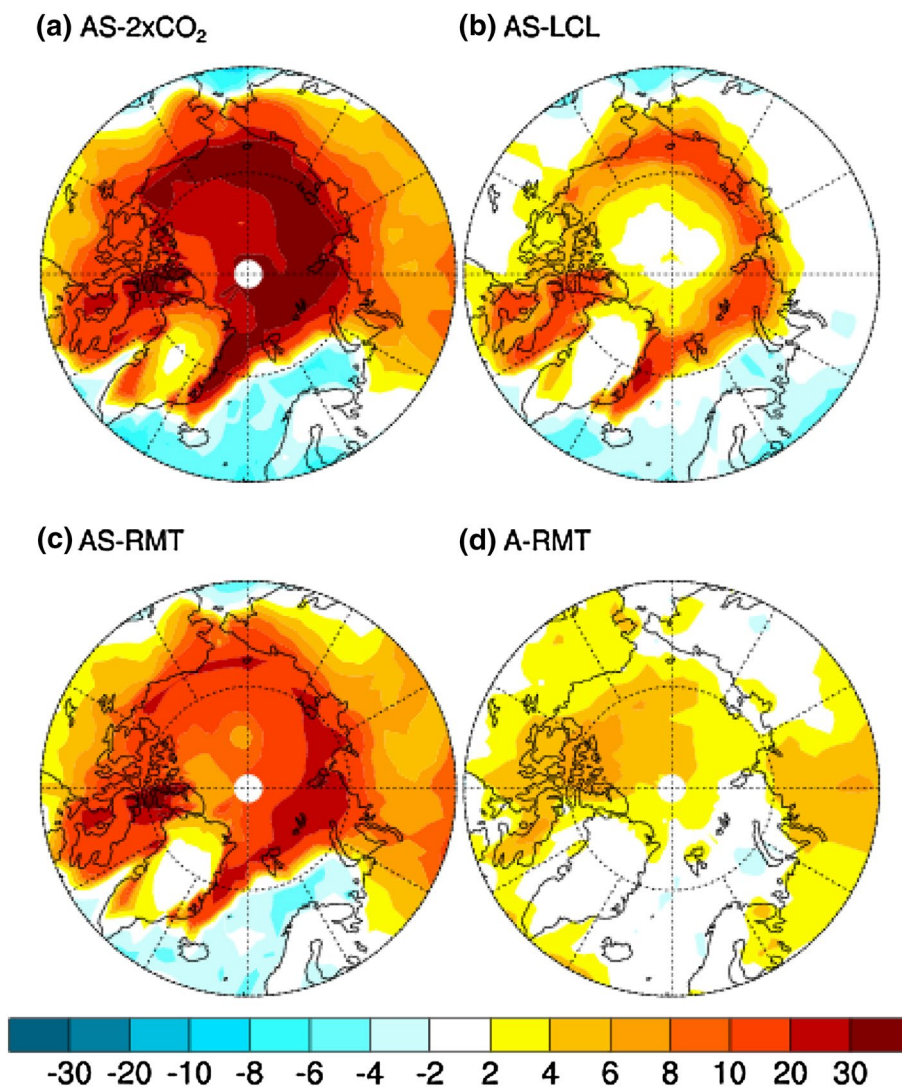
5 Discussions

The role atmospheric heat transport in the Arctic warming is discussed in many previous studies and important feedbacks identified in the current study are not new: the importance of LW water vapor and cloud feedbacks induced by poleward water vapor transport was reported by Graverson and Wang (2009); cloud feedbacks induced by sea ice reduction is emphasized by Vavrus (2004) and Yoshimori et al. (2014a); and partial cancellation of ice albedo effect by increased clouds in summer are found robust among multiple models by Crook et al. (2011) and Lu and Cai (2009b). What is new here is the approach combining the feedback suppression method (Bony et al. 2006; Stein and Alpert 1993) by prescribing the sea surface conditions not globally but regionally, and full energy budget analysis

using the CFRAM (Yoshimori et al. 2014a). By so doing, we are able to quantify relative contributions of individual feedbacks and their interactions with the atmospheric heat transport in a systematic way. While this approach provides some insight into the interaction between feedbacks, the current study is still limited to gain insight into the cause-and-effect due to the analysis of equilibrium states. For a better understanding of causal mechanisms, transient states simulated with a full ocean model must be analyzed in much the same way. The lack of ocean dynamical feedback in the current study warrants further investigation.

Our results are consistent with Chung and Räisänen (2011) in that the influence of remote surface warming is predominant in the Arctic warming, and with Screen et al. (2012) in that enhanced surface warming in the Arctic is attributed to the change in the local sea surface conditions.

Fig. 10 Changes in low-level cloud cover from the control experiments in September–October–November (%): **a** AS-2xCO₂; **b** AS-LCL; **c** AS-RMT; and **d** A-RMT



Our results are also consistent with Alexeev et al. (2005) in that the increase in the atmospheric heat transport induced by the tropical warming, rather than responding to the meridional temperature gradient, is important in the Arctic warming as well as consequent Arctic surface warming via enhanced downward LW radiation. Furthermore, our results support the explanation provided by Graversen and Burtu (2016) based on the regression analysis for the negative, rather than positive, correlation found by Hwang et al. (2011) between the Arctic amplification and atmospheric poleward heat transport across models. That is, the atmospheric heat transport represented as the sum of DSE and LH components does not provide a good measure for contribution of atmospheric dynamics to the Arctic warming. The total heat transport may be dominated by the DSE component, but the warming effect may be brought more effectively by the LH component through the consequent greenhouse effect. It is of great concern that, to the authors' best knowledge, no observational support from the ongoing

Arctic warming has been provided regarding the simulated trends in global atmospheric poleward DSE and LH transport changes. Thus, it is unclear whether or not the consistent projections among CMIP models, i.e., DSE decrease and LH increase in the future Arctic import, is even reliable at this stage.

We should note that our experimental design of regionally partitioning the forcing may have introduced an artificial meridional temperature gradient in each sensitivity experiment (AS-LCL and AS-RMT) which does not exist in the realistic simulation (AS-2xCO₂). Thus, the role of DSE response may have been overemphasized in the current study. Nevertheless, the LH transport appears to be controlled by the low-latitude warming, rather than the meridional temperature gradient. Having said that, we believe that the hybrid use of sensitivity experiments and full feedback diagnosis is a promising approach for the understanding of the complex climate system.

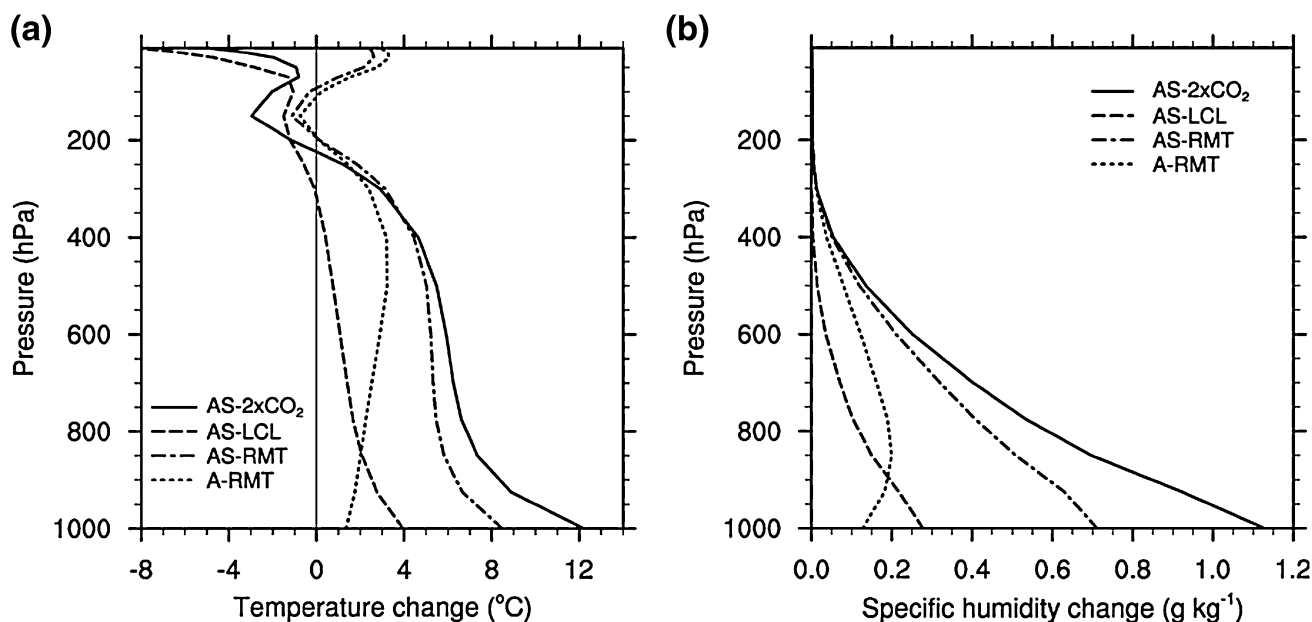


Fig. 11 Changes in atmospheric vertical profile from the control simulation in September–October–November averaged over the Arctic region ($\geq 70^\circ\text{N}$): **a** air temperature ($^\circ\text{C}$); and **b** specific humidity (g kg^{-1})

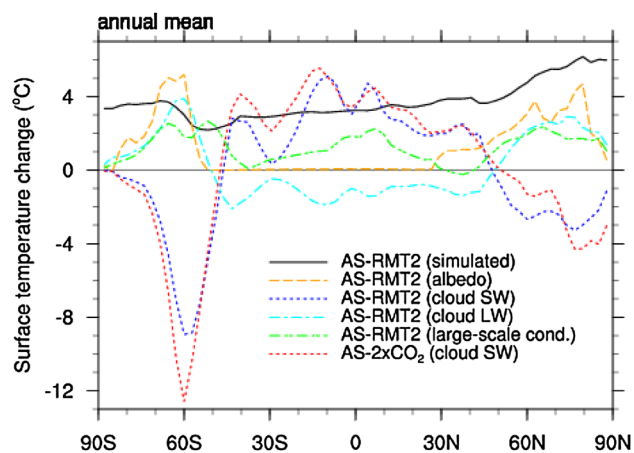


Fig. 12 Zonal and annual mean surface temperature changes with respect to the control experiments. The *black solid line* represents the simulated surface temperature change in AS-RMT2 and *other lines* represent the partial surface temperature change in AS-RMT2 or AS-2xCO₂ diagnosed using the CFRAM technique ($^\circ\text{C}$). SW and LW denote shortwave and longwave components, respectively

6 Conclusions

In previous studies, various processes have been proposed, including the ice albedo feedback, for the Arctic warming amplification and their relative contributions have been investigated to some extent using the climate feedback analysis technique (Yoshimori et al. 2014a, b). There remain some limitations, however, in such an approach for the understanding of the interaction of feedbacks and the

mechanism of Arctic warming. In order to elucidate how the extra-Arctic warming remotely influences the Arctic warming, we conducted sensitivity experiments which isolate the remote and local effect by using an atmospheric GCM with thermally interactive and non-interactive ocean mixed layer depending on the region. The effect of ocean circulation change is not considered here. The resulting Arctic warming is generally larger when the model is forced by the remote surface warming, rather than responding to the local CO₂ radiative forcing. This indicates that much of the Arctic warming under elevated CO₂ levels is induced by the low latitude warming via the increased atmospheric heat transport. The combination of the sensitivity experiments and climate feedback analysis reveals the role of atmospheric heat transport and regional feedbacks in the Arctic warming.

A summary of the effect of remote surface warming on the Arctic surface warming based on the A-RMT experiment is provided schematically in Fig. 13. The warming outside of the NH mid-high latitudes tends to increase the Arctic import of DSE and LH. The DSE import to the Arctic directly warms the atmosphere and the LH import to the Arctic warms the atmosphere through condensation. The resultant Arctic atmospheric warming with fixed sea surface conditions tends to reduce the surface evaporation. Additionally, the LH or water vapor transport increases the greenhouse effect of water vapor and clouds. For this reason, total heat (MSE) transport of the atmosphere may not be a good proxy to measure the contribution of atmospheric dynamics to the Arctic warming.

Fig. 13 Schematic diagram of feedback processes in A-RMT based on the CFRAM analysis. Upward and downward arrows indicate increase and decrease, respectively. Note that only selected processes are shown

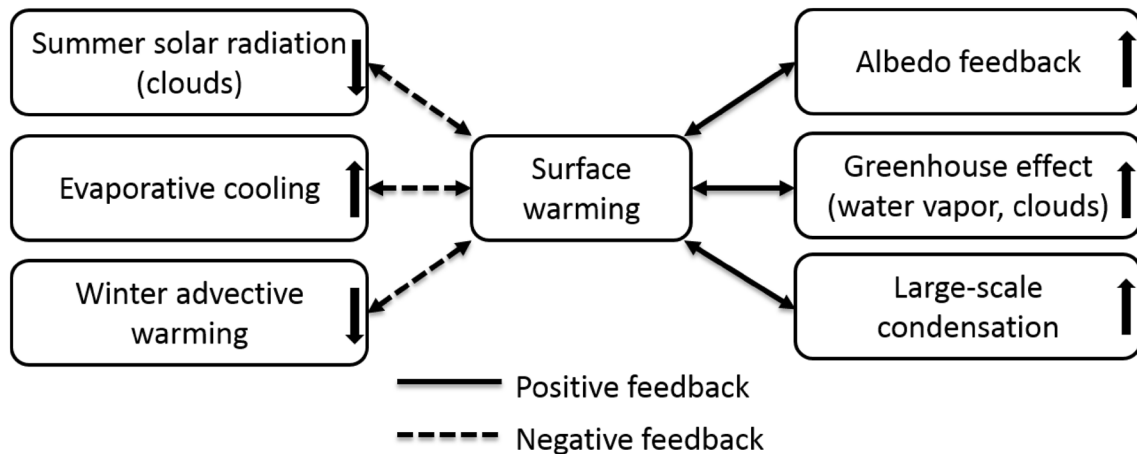
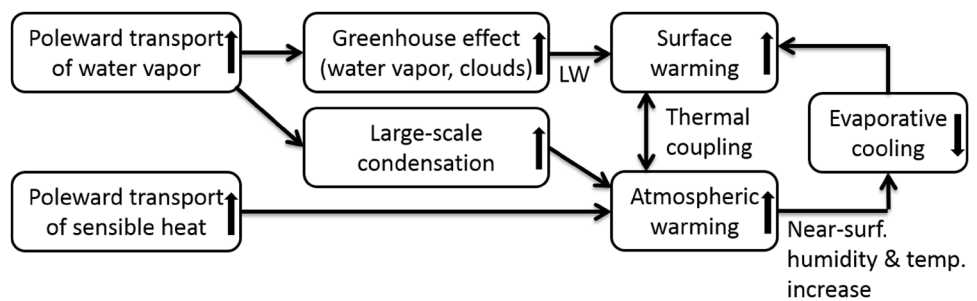


Fig. 14 Schematic diagram of feedback processes induced by the surface warming in the Arctic based on the difference between AS-RMT and A-RMT CFRAM analysis. Upward and downward arrows

indicate increase and decrease, respectively. Note that only selected processes are shown

A summary for the regional feedbacks induced by the Arctic surface warming based on the AS-RMT and AS-LCL is provided schematically in Fig. 14. Surface warming induces the positive albedo feedback, but it is partially counteracted by the sun-shade effect of clouds in summer. In winter, surface warming induces the negative feedback of increased evaporative cooling, but it is counteracted by the increased greenhouse effect of water vapor and clouds and increased large-scale condensation. Advective warming responds to the surface warming negatively through the reduced DSE transport under the weakened meridional temperature gradient.

While the poleward atmospheric heat transport was relatively symmetric between the NH and SH high latitudes, the asymmetric polar warming occurs even in the equilibrium response to the CO₂ increase without ocean dynamics. The SW cloud feedback associated with solid to liquid state conversion of cloud condensate was attributed to be the main cause for this asymmetry. It is thus suggested that the model representation of clouds and cloud response to the global warming over the Southern Ocean play important roles in determining the meridional structure of the atmospheric warming at the global scale.

Acknowledgements We thank two anonymous reviewers for their useful suggestions. All experiments were carried out using the NIES supercomputer system except for a pair of bipolar experiments which were conducted with the JAMSTEC Earth Simulator 3. We are thankful to the MIROC model developing team. We thank developers of freely available software, NCL. This research was supported by the GRENE Arctic Climate Change Research Project and the Environment Research and Technology Development Fund (S-10) of the Japanese Ministry of the Environment.

References

Alexeev VA, Langen PL, Bates JR (2005) Polar amplification of surface warming on an aquaplanet in “ghost forcing” experiments without sea ice feedbacks. *Clim Dyn* 24:655–666. doi:10.1007/s00382-005-0018-3

Alexeev VA, Esau I, Polyakov IV, Byam SJ, Sorokina S (2012) Vertical structure of recent arctic warming from observed data and reanalysis products. *Clim Change* 111:215–239. doi:10.1007/s10584-011-0192-8

Armour KC, Marshall J, Scott JR, Donohoe A, Newsom ER (2016) Southern Ocean warming delayed by circumpolar upwelling and equatorward transport. *Nat Geosci* 9:549–554. doi:10.1038/ngeo2731

Bitz CM, Fu Q (2008) Arctic warming aloft is data set dependent. *Nature* 455:E3–E4. doi:10.1038/nature07258

- Bony S, Colman R, Kattsov VM, Allan RP, Bretherton CS, Dufresne JL, Hall A, Hallegatte S, Holland MM, Ingram W, Randall DA, Soden BJ, Tselioudis G, Webb MJ (2006) How well do we understand and evaluate climate change feedback processes? *J Clim* 19:3445–3482. doi:[10.1175/jcli3819.1](https://doi.org/10.1175/jcli3819.1)
- Cai M (2005) Dynamical amplification of polar warming. *Geophys Res Lett* 32, Artn L22710. doi:[10.1029/2005gl024481](https://doi.org/10.1029/2005gl024481)
- Cai M, Lu JH (2009) A new framework for isolating individual feedback processes in coupled general circulation climate models. Part II: method demonstrations and comparisons. *Clim Dyn* 32:887–900. doi:[10.1007/s00382-008-0424-4](https://doi.org/10.1007/s00382-008-0424-4)
- Chung CE, Räisänen P (2011) Origin of the Arctic warming in climate models. *Geophys Res Lett* 38. doi:[10.1029/2011gl049816](https://doi.org/10.1029/2011gl049816)
- Crook JA, Forster PM, Stuber N (2011) Spatial patterns of modeled climate feedback and contributions to temperature response and polar amplification. *J Clim* 24:3575–3592. doi:[10.1175/2011jcli3863.1](https://doi.org/10.1175/2011jcli3863.1)
- Grant AN, Bronnimann S, Haimberger L (2008) Recent Arctic warming vertical structure contested. *Nature* 455:E2–E3. doi:[10.1038/nature07257](https://doi.org/10.1038/nature07257)
- Graversen RG, Burtu M (2016) Arctic amplification enhanced by latent energy transport of atmospheric planetary waves. *Q J R Meteorol Soc* 142:2046–2054. doi:[10.1002/qj.2802](https://doi.org/10.1002/qj.2802)
- Graversen RG, Wang MH (2009) Polar amplification in a coupled climate model with locked albedo. *Clim Dyn* 33:629–643. doi:[10.1007/s00382-009-0535-6](https://doi.org/10.1007/s00382-009-0535-6)
- Graversen RG, Mauritsen T, Tjernstrom M, Kallen E, Svensson G (2008) Vertical structure of recent Arctic warming. *Nature* 451:53–56. doi:[10.1038/nature06502](https://doi.org/10.1038/nature06502)
- Holland MM, Bitz CM (2003) Polar amplification of climate change in coupled models. *Clim Dyn* 21:221–232. doi:[10.1007/s00382-003-0332-6](https://doi.org/10.1007/s00382-003-0332-6)
- Hwang YT, Frierson DMW, Kay JE (2011) Coupling between Arctic feedbacks and changes in poleward energy transport. *Geophys Res Lett* 38, Artn L17704. doi:[10.1029/2011gl048546](https://doi.org/10.1029/2011gl048546)
- Keith DW (1995) Meridional energy-transport—uncertainty in zonal means. *Tellus Ser A Dyn Meteorol Oceanogr* 47:30–44. doi:[10.1034/j.1600-0870.1995.00002.x](https://doi.org/10.1034/j.1600-0870.1995.00002.x)
- Laine A, Nakamura H, Nishii K, Miyasaka T (2014) A diagnostic study of future evaporation changes projected in CMIP5 climate models. *Clim Dyn* 42:2745–2761. doi:[10.1007/s00382-014-2087-7](https://doi.org/10.1007/s00382-014-2087-7)
- Laîné A, Yoshimori M, Abe-Ouchi A (2016) Surface Arctic amplification factors in CMIP5 models: land and oceanic surfaces, seasonality. *J Clim* 29:3297–3316. doi:[10.1175/JCLI-D-15-0497.1](https://doi.org/10.1175/JCLI-D-15-0497.1)
- Lu JH, Cai M (2009a) A new framework for isolating individual feedback processes in coupled general circulation climate models. Part I: formulation. *Clim Dyn* 32:873–885. doi:[10.1007/s00382-008-0425-3](https://doi.org/10.1007/s00382-008-0425-3)
- Lu JH, Cai M (2009b) Seasonality of polar surface warming amplification in climate simulations. *Geophys Res Lett* 36. doi:[10.1029/2009gl040133](https://doi.org/10.1029/2009gl040133), Artn L16704
- Lu JH, Cai M (2010) Quantifying contributions to polar warming amplification in an idealized coupled general circulation model. *Clim Dyn* 34:669–687. doi:[10.1007/s00382-009-0673-x](https://doi.org/10.1007/s00382-009-0673-x)
- Mahlstein I, Knutti R (2011) Ocean heat transport as a cause for model uncertainty in projected arctic warming. *J Clim* 24:1451–1460. doi:[10.1175/2010jcli3713.1](https://doi.org/10.1175/2010jcli3713.1)
- Marshall J, Armour KC, Scott JR, Kostov Y, Hausmann U, Ferreira D, Shepherd TG, Bitz CM (2014) The ocean's role in polar climate change: asymmetric Arctic and Antarctic responses to greenhouse gas and ozone forcing. *Philos Trans R Soc A Math Phys Eng Sci* 372:17. doi:[10.1098/rsta.2013.0040](https://doi.org/10.1098/rsta.2013.0040)
- Meehl GA, Covey C, Delworth T, Latif M, McAvaney B, Mitchell JFB, Stouffer RJ, Taylor KE (2007) The WCRP CMIP3 multimodel dataset—a new era in climate change research. *Bull Am Meteorol Soc* 88:1383. doi:[10.1175/Bams-88-9-1383](https://doi.org/10.1175/Bams-88-9-1383)
- Ogura T, Emori S, Webb MJ, Tsushima Y, Yokohata T, Abe-Ouchi A, Kimoto M (2008a) Towards understanding cloud response in atmospheric GCMs: the use of tendency diagnostics. *J Meteorol Soc Jpn* 86:69–79. doi:[10.2151/jmsj.86.69](https://doi.org/10.2151/jmsj.86.69)
- Ogura T, Webb MJ, Bodas-Salcedo A, Williams KD, Yokohata T, Wilson DR (2008b) Comparison of cloud response to CO₂ doubling in two GCMs. *Sola* 4:29–32. doi:[10.2151/sola.2008-008](https://doi.org/10.2151/sola.2008-008)
- Screen JA, Simmonds I (2011) Erroneous arctic temperature trends in the ERA-40 reanalysis: a closer look. *J Clim* 24:2620–2627. doi:[10.1175/2010jcli4054.1](https://doi.org/10.1175/2010jcli4054.1)
- Screen JA, Deser C, Simmonds I (2012) Local and remote controls on observed Arctic warming. *Geophys Res Lett* 39, Artn L10709. doi:[10.1029/2012gl051598](https://doi.org/10.1029/2012gl051598)
- Sejas SA, Cai M, Hu AX, Meehl GA, Washington W, Taylor PC (2014) Individual feedback contributions to the seasonality of surface warming. *J Clim* 27:5653–5669. doi:[10.1175/Jcli-D-13-00658.1](https://doi.org/10.1175/Jcli-D-13-00658.1)
- Soden BJ, Held IM, Colman R, Shell KM, Kiehl JT, Shields CA (2008) Quantifying climate feedbacks using radiative kernels. *J Clim* 21:3504–3520. doi:[10.1175/2007jcli2110.1](https://doi.org/10.1175/2007jcli2110.1)
- Solomon A (2006) Impact of latent heat release on polar climate. *Geophys Res Lett* 33. doi:[10.1029/2005gl025607](https://doi.org/10.1029/2005gl025607)
- Stein U, Alpert P (1993) Factor separation in numerical simulations. *J Atmos Sci* 50:2107–2115. doi:[10.1175/1520-0469\(1993\)050<2.0.Co;2](https://doi.org/10.1175/1520-0469(1993)050<2.0.Co;2)
- Taylor KE, Stouffer RJ, Meehl GA (2012) An overview of Cmp5 and the experiment design. *Bull Am Meteorol Soc* 93:485–498. doi:[10.1175/Bams-D-11-00094.1](https://doi.org/10.1175/Bams-D-11-00094.1)
- Taylor PC, Cai M, Hu A, Meehl J, Washington W, Zhang GJ (2013) A decomposition of feedback contributions to polar warming amplification. *J Clim* 26:7023–7043. doi:[10.1175/jcli-d-12-00696.1](https://doi.org/10.1175/jcli-d-12-00696.1)
- Thorne PW (2008) Arctic tropospheric warming amplification? *Nature* 455:E1–E2. doi:[10.1038/nature07256](https://doi.org/10.1038/nature07256)
- Tsushima Y, Emori S, Ogura T, Kimoto M, Webb MJ, Williams KD, Ringer MA, Soden BJ, Li B, Andronova N (2006) Importance of the mixed-phase cloud distribution in the control climate for assessing the response of clouds to carbon dioxide increase: a multi-model study. *Clim Dyn* 27:113–126. doi:[10.1007/s00382-006-0127-7](https://doi.org/10.1007/s00382-006-0127-7)
- Vavrus S (2004) The impact of cloud feedbacks on Arctic climate under greenhouse forcing. *J Clim* 17:603–615. doi:[10.1175/1520-0442\(2004\)017<2.0.Co;2](https://doi.org/10.1175/1520-0442(2004)017<2.0.Co;2)
- Yoshimori M, Yokohata T, Abe-Ouchi A (2009) A comparison of climate feedback strength between CO₂ doubling and LGM experiments. *J Clim* 22:3374–3395. doi:[10.1175/2009jcli2801.1](https://doi.org/10.1175/2009jcli2801.1)
- Yoshimori M, Abe-Ouchi A, Watanabe M, Oka A, Ogura T (2014a) Robust seasonality of Arctic warming processes in two different versions of the MIROC GCM. *J Clim* 27:6358–6375. doi:[10.1175/jcli-d-14-00086.1](https://doi.org/10.1175/jcli-d-14-00086.1)
- Yoshimori M, Watanabe M, Abe-Ouchi A, Shiogama H, Ogura T (2014b) Relative contribution of feedback processes to Arctic amplification of temperature change in MIROC GCM. *Clim Dyn* 42:1613–1630. doi:[10.1007/s00382-013-1875-9](https://doi.org/10.1007/s00382-013-1875-9)
- Yoshimori M, Watanabe M, Shiogama H, Oka A, Abe-Ouchi A, Ohgaito R, Kamae Y (2016) A review of progress towards understanding the transient global mean surface temperature response to radiative perturbation. *Prog Earth Planet Sci* 3:1–14. doi:[10.1186/s40645-016-0096-3](https://doi.org/10.1186/s40645-016-0096-3)